# High-energy above-threshold detachment from negative ions

A. Gazibegović-Busuladžić,[1] D. B. Milošević,[1] and W. Becker[2]
[1]*Faculty of Science, University of Sarajevo, Zmaja od Bosne 35, 71000 Sarajevo, Bosnia and Herzegovina*
[2]*Max-Born-Institut, Max-Born-Strasse 2a, 12489 Berlin, Germany*
(Received 24 July 2004; published 10 November 2004)

Above-threshold detachment of electrons from negative ions by an elliptically polarized laser field is analyzed within the strong-field approximation. The low-energy part of the spectrum, that is, its structure and its apparent cutoff, strongly depends on the orbital quantum number $l$ of the initial ground state. The high-energy part is characterized by the usual extended plateau caused by rescattering, which is essentially independent of the ground state. The potential that the returning electron experiences during rescattering is modeled by the sum of a polarization potential and a static potential. This rescattering potential does not have much effect on the shape of the plateau, but it does on its height. For $H^-$ ($l=0$), the yield of rescattered electrons is five orders of magnitude below the direct electrons, while for $I^-$ ($l=1$) the yields only differ by a factor of 40. We also analyze the dependence of the angle-resolved energy spectrum on the ellipticity of the laser field and confirm general symmetry properties. An angle-integrated elliptic dichroism parameter is introduced and analyzed.

DOI: 10.1103/PhysRevA.70.053403 PACS number(s): 32.80.Rm, 42.65.Re, 42.50.Hz

## I. INTRODUCTION

Laser-induced above-threshold detachment (ATD) of negatively charged ions differs from above-threshold ionization (ATI) of neutral atoms by the absence of the net Coulomb attraction of the detached electron by the residual atom. Since the outermost electron of a negatively charged ion is only loosely bound and easily detached by moderately strong fields, it has been a challenge for many years to carry out experiments with negatively charged ions with fields strong enough to observe the nonperturbative effects that are characteristic of ATI [1]. The early strong-field experiments only investigated total detachment rates [2]. Only recent measurements have succeeded in recording angle-resolved energy spectra for $H^-$ [3] and, thereafter, for $F^-$ [4]. The rescattering regime [5], which has generated the strong renewed interest in ATI over the past decade, has not yet been entered in ATD, even though the recent experiment [4] came close.

Strong-field ionization of many-electron atoms can be remarkably well described in the single-active-electron approximation (SAEA), where the problem is treated as an effective one-electron problem with an optimized atom-specific one-electron potential. Numerical solutions of the three-dimensional time-dependent Schrödinger equation in this context have reproduced the experimentally observed angular-resolved electron energy spectra with high accuracy [6,7]. However, for an elliptically polarized laser field, especially if the intensity is high and the frequency in the infrared, this method becomes extremely time consuming.

Within the SAEA, ATI processes have been successfully described using quantum-mechanical models based on the strong-field approximation (SFA) [8], which yields excellent agreement with the data, in particular for circular polarization and not too low electron energies [9]. The high-order ATI spectrum is characterized by an extended plateau whose height is several orders of magnitude lower than that of the direct ATI spectrum and extends up to a well-defined cutoff. This plateau is the manifestation of rescattering [10]. It is very well described by an improved Keldysh-Faisal-Reiss (KFR) theory that takes into account the first-order correction in the rescattering potential [11,12]. The elastic or inelastic recollision of the ionized electron with its parent ion leads to a variety of processes. Besides high-order ATI [13–15], these include high-order harmonic generation [16], nonsequential multiple ionization [17], laser-assisted x-ray atom scattering [18], electron-ion recombination [19], and electron-atom scattering [20].

The main problem of the SFA applied to ATI is its neglect of the Coulomb attraction between the ionized electron and its parent ion. This affects, in particular, the total ionization rate and the electron spectrum for low energies, especially for elliptic polarization. Moreover, even the improved SFA does not incorporate the important effect of Coulomb refocusing of the wave packet of the returning electron [21]. Consequently, one may also question its reliability regarding high-order ATI, even though, for reasons not fully understood, it reproduces even subtle effects such as the intensity-dependent enhancements of groups of ATI peaks [22,23].

This problem is absent from ATD, and indeed it has been argued that the combined SAEA and SFA should be quantitatively reliable in this realm [24]. This has been recently confirmed for the negative ion $H^-$ [3,25,26]. In particular, given the absence of Coulomb refocusing, the improved SFA should yield excellent results when applied to high-order ATD of the negative ions. On the experimental side, there is the problem of how to prevent premature detachment in the leading edge of the pulse, in view of the low electron affinity of the negative ions. This can be accomplished with the help of short pulses and/or low frequencies, and by a proper choice of the ion. The maximum binding energy is realized by negative ions with a filled valence shell [27]. The electron affinity of halogen ions (such as $F^-$) exceeds 3 eV and therefore they are most suitable to explore strong-field effects experimentally. Experiments with heavier halogen ions ($Cl^-$, $Br^-$, and $I^-$) have been done, but only for few-photon detachment (see, for example, [28] and references therein).

With this in mind, we focus in this paper on high-order ATD of negative ions, in particular for an elliptically polar-

 

ized laser field. We will use the SFA formalism similar to that of Ref. [12] in which high-order ATI by a linearly polarized laser field was considered. The difference is the absence of the long-range Coulomb potential. Also, for rescattering we will use optimally suited potentials that depend on the electronic structure of the respective ion. Preliminary results of this approach have been communicated before [29], also with regard to the experiment [4].

In the absence of the long-range Coulomb potential, a useful model results when the remaining electron-core interaction is modeled by a zero-range potential. This permits an accurate solution within the quasistationary quasienergy approach [30,31]; for a review, see Ref. [32]. The ground states of negative ions with high electron affinity (such as $F^-$, $Cl^-$, $Br^-$, $I^-$, $At^-$) are $p$ states ($l=1$), while the standard zero-range potential approach was developed for $s$ states ($l=0$). Recently, the effective-range method was applied in this context [33], and the results were compared [34] with the experiment [4].

The generalization of the SFA to elliptic polarization is straightforward, thanks to the availability of the Volkov solution [35]. However, this theory produces a fourfold symmetry in the angle-resolved electron spectra, which is strongly violated by the experimental data for low electron energies. Taking rescattering into account [36], which disobeys the fourfold symmetry, does not improve the agreement, since its effect on the low-energy spectra is insignificant. Much work has been done in order to explain these results (see references in [14]). Again, for negative ions the SFA results for elliptical polarization are expected to be reliable, but a verification is still needed.

In the present paper, we will analyze the ellipticity dependence of the angular distributions of electrons with $s$ and $p$ initial-state symmetry. Particular attention will be devoted to the dependence of this angular distribution on the sign of the ellipticity (the so-called elliptic dichroism effect [37]). We use the atomic system of units ($\hbar=e=m=1$).

## II. THEORY

Consider a negative ion initially in its ground state $|\psi_i\rangle$ that is irradiated by a laser pulse with vector potential $\mathbf{A}(t)$ and electric field $\mathbf{E}(t)=-d/dt\mathbf{A}(t)$. The probability amplitude for detecting an ATD electron with momentum $\mathbf{p}$ and kinetic energy $E_\mathbf{p}=\mathbf{p}^2/2$ is [14]

$$M_{\mathbf{p}i}=-i\lim_{t\to\infty}\int_{-\infty}^{t}dt'\langle\psi_\mathbf{p}(t)|U(t,t')\mathbf{r}\cdot\mathbf{E}(t')|\psi_i(t')\rangle. \quad (1)$$

Here $U(t,t')$ is the time-evolution operator of the Hamiltonian

$$H(t)=-\frac{\boldsymbol{\nabla}^2}{2}+\mathbf{r}\cdot\mathbf{E}(t)+V(\mathbf{r}), \quad (2)$$

where $\mathbf{r}\cdot\mathbf{E}(t)$ is the laser-field–electron interaction in the length gauge and the dipole approximation, and $V(\mathbf{r})$ is the interaction of the electron with the rest of the negative ion in the absence of the laser field. The states $\psi_\mathbf{p}$ and $\psi_i$ are a scattering state with asymptotic momentum $\mathbf{p}$ and the ground state, respectively, of the negative-ion Hamiltonian $H_i=-\boldsymbol{\nabla}^2/2+V(\mathbf{r})$. The time-evolution operator $U(t,t')$ satisfies the Dyson equation

$$U(t,t')=U_\mathrm{L}(t,t')-i\int_{t'}^{t}dt''U_\mathrm{L}(t,t'')VU(t'',t'), \quad (3)$$

where $U_\mathrm{L}(t,t')$ is the time-evolution operator of the Hamiltonian $H_\mathrm{L}(t)=-\boldsymbol{\nabla}^2/2+\mathbf{r}\cdot\mathbf{E}(t)$ of a free electron in the laser field. The eigenstates of the time-dependent Schrödinger equation with the Hamiltonian $H_\mathrm{L}(t)$ are the Volkov states

$$|\psi_\mathbf{p}^{(\mathrm{L})}(t)\rangle=|\mathbf{p}+\mathbf{A}(t)\rangle\exp[-iS_\mathbf{p}(t)], \quad (4)$$

where

$$S_\mathbf{p}(t)=\frac{1}{2}\int^{t}dt'[\mathbf{p}+\mathbf{A}(t')]^2, \quad (5)$$

and $|\mathbf{q}\rangle$ denotes a plane-wave state [$\langle\mathbf{r}|\mathbf{q}\rangle=(2\pi)^{-3/2}\exp(i\mathbf{q}\cdot\mathbf{r})$]. The Volkov time-evolution operator has the expansion

$$U_\mathrm{L}(t,t')=\int d^3\mathbf{k}|\psi_\mathbf{k}^{(\mathrm{L})}(t)\rangle\langle\psi_\mathbf{k}^{(\mathrm{L})}(t')|. \quad (6)$$

Equations (1) and (3) are exact. Introducing the strong-field approximation, i.e., replacing $\langle\psi_\mathbf{p}(t)|U(t,t')$ with $\langle\psi_\mathbf{p}^{(\mathrm{L})}(t)|U(t,t')$ in Eq. (1) and, subsequently, $U$ with $U_\mathrm{L}$ on the right-hand side of Eq. (3), we get

$$M_{\mathbf{p}i}^{\mathrm{SFA}}=M_{\mathbf{p}i}^{(0)}+M_{\mathbf{p}i}^{(1)}, \quad (7)$$

where

$$M_{\mathbf{p}i}^{(0)}=-i\int_{-\infty}^{\infty}dt\langle\psi_\mathbf{p}^{(\mathrm{L})}(t)|\mathbf{r}\cdot\mathbf{E}(t)|\psi_i(t)\rangle, \quad (8)$$

$$M_{\mathbf{p}i}^{(1)}=-\int_{-\infty}^{\infty}dt\int_{t}^{\infty}dt'\langle\psi_\mathbf{p}^{(\mathrm{L})}(t')|VU_\mathrm{L}(t',t)\mathbf{r}\cdot\mathbf{E}(t)|\psi_i(t)\rangle. \quad (9)$$

The amplitude $M_{\mathbf{p}i}^{(0)}$ is the KFR amplitude [8], which describes direct electron detachment [24], while the amplitude $M_{\mathbf{p}i}^{(1)}$ is the rescattering amplitude, which is responsible for the high-energy plateau in the electron energy spectrum. It corresponds to a generalization of the three-step model of high-order above-threshold ionization (see [14] and references therein) to high-order ATD. In the first step, the electron is detached from the negative ion; in the second step, the free electron moves in the laser field and may return to the atom; in the third step, the electron scatters elastically off the atom. Owing to further acceleration after this elastic scattering, the electron can acquire an energy much higher than in the direct ATD process. In principle, in the single-active-electron approximation, the potential $V(\mathbf{r})$ represents the optimized one-particle potential felt by the electron. We will discuss our choice of $V(\mathbf{r})$ in Appendixes C and D.

Using partial integration and the Schrödinger equations for functions $\psi_{\mathbf{p}}^{(\mathrm{L})}$ and $\psi_i(t)=\psi_i \exp(-iE_i t)$, the amplitude $M_{\mathbf{p}i}^{(0)}$ can be transformed into

$$M_{\mathbf{p}i}^{(0)} = i\int_{-\infty}^{\infty} dt \left\{ \frac{[\mathbf{p}+\mathbf{A}(t)]^2}{2} - E_i \right\} \langle \psi_{\mathbf{p}}^{(\mathrm{L})}(t) | \psi_i(t) \rangle, \quad (10)$$

where $E_i$ is the energy of the ground state. Inserting Eq. (6) into Eq. (9) and performing the integration over the intermediate electron momenta $\mathbf{k}$ (see Appendix A), we get the following exact result ($t'=t-\tau$):

$$M_{\mathbf{p}i}^{(1)} = -\int_{-\infty}^{\infty} dt \int_0^{\infty} d\tau \left(\frac{2\pi}{i\tau}\right)^{3/2} \exp\{i[S_{\mathbf{k}_s}(t') - S_{\mathbf{k}_s}(t)]\}$$
$$\times \exp\left(-\frac{i}{2\tau}\frac{\partial^2}{\partial \mathbf{k}^2}\right) \langle \psi_{\mathbf{p}}^{(\mathrm{L})}(t) | V | \mathbf{k}+\mathbf{A}(t) \rangle$$
$$\times \langle \mathbf{k}+\mathbf{A}(t') | \mathbf{r}\cdot\mathbf{E}(t') | \psi_i(t') \rangle \big|_{\mathbf{k}=\mathbf{k}_s}, \quad (11)$$

where

$$\mathbf{k}_s = -\frac{1}{\tau}\int_{t-\tau}^{t} dt' \mathbf{A}(t') = \frac{1}{\tau}[\boldsymbol{\alpha}(t-\tau) - \boldsymbol{\alpha}(t)], \quad (12)$$

with $\boldsymbol{\alpha}(t)=\int^t dt' \mathbf{A}(t')$.

Exploiting the periodicity of the laser field with respect to $T=2\pi/\omega$, as in Ref. [12], we can decompose the transition amplitude in the form

$$M_{\mathbf{p}i} = -2\pi i \sum_n \delta(E_{\mathbf{p}} - E_i + U_{\mathrm{p}} - n\omega) T_{\mathbf{p}i}(n), \quad (13)$$

which also displays energy conservation in terms of "absorption of laser photons." The differential detachment with absorption of $n$ photons is then

$$w_{\mathbf{p}i}(n) = 2\pi p |T_{\mathbf{p}i}(n)|^2. \quad (14)$$

In the expressions above, we defined

$$T_{\mathbf{p}i}(n) = \int_0^{2\pi} \frac{d\varphi}{2\pi} \mathcal{T}_{\mathbf{p}i}(\varphi) \exp(in\varphi), \quad (15)$$

where ( $\varphi=\omega t$, $\varphi'=\varphi-\omega\tau$)

$$\mathcal{T}_{\mathbf{p}i}(\varphi) = (\mathcal{T}_{\mathbf{p}i}^{(0)} + \mathcal{T}_{\mathbf{p}i}^{(1)}) \exp\{i[\mathbf{p}\cdot\boldsymbol{\alpha}(\varphi) + \mathcal{U}_1(\varphi)]\}, \quad (16)$$

with $[\mathbf{q}=\mathbf{p}+\mathbf{A}(\varphi)]$,

$$\mathcal{T}_{\mathbf{p}i}^{(0)}(\varphi) = i\mathbf{E}(\varphi)\cdot\frac{\partial}{\partial \mathbf{q}} \tilde{\psi}_i(\mathbf{q}) = \left(E_i - \frac{\mathbf{q}^2}{2}\right)\tilde{\psi}_i(\mathbf{q}), \quad (17)$$

$$\mathcal{T}_{\mathbf{p}i}^{(1)}(\varphi) = -i\int_0^{\infty} d\tau \left(\frac{2\pi}{i\tau}\right)^{3/2} \exp\{i[S_{\mathbf{k}_s}(\varphi') - S_{\mathbf{k}_s}(\varphi)$$
$$+ E_i\tau]\} \exp\left(-\frac{i}{2\tau}\frac{\partial^2}{\partial \mathbf{k}^2}\right) V_{\mathbf{k}-\mathbf{p}} \langle \mathbf{k}+\mathbf{A}(\varphi') | \mathbf{r}\cdot\mathbf{E}(\varphi')$$
$$\times |\psi_i\rangle \big|_{\mathbf{k}=\mathbf{k}_s}, \quad (18)$$

$$\tilde{\psi}_i(\mathbf{q}) = \int \frac{d^3\mathbf{r}}{(2\pi)^{3/2}} \psi_i(\mathbf{r}) \exp(-i\mathbf{q}\cdot\mathbf{r}), \quad (19)$$

$$V_{\mathbf{K}} = \int \frac{d^3\mathbf{r}}{(2\pi)^3} V(\mathbf{r}) \exp(i\mathbf{K}\cdot\mathbf{r}). \quad (20)$$

The function $\mathcal{U}_1(\varphi)$ in Eq. (16) is defined as the periodic part of $\mathcal{U}(t)=\frac{1}{2}\int^t dt' \mathbf{A}^2(t') = \mathcal{U}_1(t) + U_{\mathrm{P}} t$, with $U_{\mathrm{P}}$ the ponderomotive energy. The terms $\mathcal{T}_{\mathbf{p}i}^{(0)}$ and $\mathcal{T}_{\mathbf{p}i}^{(1)}$ correspond to detachment without and with rescattering, respectively. The integral over the travel time $\tau$ in Eq. (18) can be done by numerical integration, while the integral over $\varphi$ in Eq. (15) can be performed using the fast Fourier transform, or also by numerical integration. The integrands contain matrix elements whose explicit form is given in Appendixes B, C, and E.

Alternatively, the integrals over time in the above equations can be evaluated by the method of steepest descent (saddle-point method). The results in this paper will be obtained as described above, but for later use in Sec. IV C we state here the "saddle-point equation"

$$[\mathbf{p}+\mathbf{A}(t)]^2 = 2E_i. \quad (21)$$

This equation is obtained by looking for times $t$ that render the exponential under the integral on the right-hand side of Eq. (10) or Eq. (15) with Eqs. (16) and (17) stationary. This exponential receives contributions from the Volkov action (5) and the bound-state energy, which immediately leads to the condition (21). Since $E_i<0$, the solutions $t_s$ will be complex. With the action (5) evaluated at the saddle-point solutions, the direct amplitude assumes the form

$$T_{\mathbf{p}i}^{(0)}(n) = -\frac{1}{2T}\sum_s \left[\frac{2\pi}{iS_{\mathbf{p}}''(t_s)}\right]^{1/2} \exp[iS_{\mathbf{p}i}(t_s)]$$
$$\times \{[\mathbf{p}+\mathbf{A}(t_s)]^2 - 2E_i\} \tilde{\psi}_i(\mathbf{p}+\mathbf{A}(t_s)), \quad (22)$$

where $S_{\mathbf{p}i}(t)=S_{\mathbf{p}}(t)-E_i t$, $S_{\mathbf{p}}''(t)=-\mathbf{E}(t)\cdot[\mathbf{p}+\mathbf{A}(t)]$.

## III. SYMMETRY CONSIDERATIONS

We will present explicit results for the elliptically polarized laser field

$$\mathbf{E}(t) = \frac{E_{\mathrm{L}}}{\sqrt{1+\varepsilon^2}}(\hat{\mathbf{e}}_z \sin\omega t - \hat{\mathbf{e}}_y \varepsilon \cos\omega t) \quad (23)$$

with ellipticity $\varepsilon$, where $\hat{\mathbf{e}}_y$ and $\hat{\mathbf{e}}_z$ are the unit polarization vectors along the $y$ and $z$ axis, respectively. For the momentum of the detached electron, we use spherical coordinates $\mathbf{p}=(p,\theta,\phi)$ with the polar axis in the direction of the semimajor axis of the field (23) so that $\cos\theta=\hat{\mathbf{p}}\cdot\hat{\mathbf{e}}_z$. The electron momentum is in the polarization plane of the laser if $\phi=\pm\pi/2$.

The exact differential ionization rate $w(\mathbf{p},\varepsilon)\equiv w_{\mathbf{p}i}(n)$ [38] satisfies the inversion symmetry (twofold symmetry) [39]

$$w(-\mathbf{p},\varepsilon) = w(\mathbf{p},\varepsilon), \quad (24)$$

as well as the symmetry

$$w(\mathbf{p},-\varepsilon) = w(p_x,-p_y,p_z,\varepsilon) = w(p_x,p_y,-p_z,\varepsilon). \quad (25)$$

The symmetry (24) corresponds to $(\theta,\phi) \rightarrow (\pi-\theta,\phi+\pi)$, while for Eq. (25) $p_y \rightarrow -p_y$ implies

$\phi \to \phi + \pi$, and $p_z \to -p_z$ corresponds to $\theta \to \pi - \theta$. In addition, the rate is independent of the sign of the momentum component $p_x$ which is perpendicular to the plane of polarization.

If we consider only electron emission within the polarization plane, it is convenient to introduce the polar coordinates $(p, \psi)$ in the $yz$ plane, such that $\tan \psi = p_y/p_z$, where $\psi$ is the angle with respect to the major axis of the polarization ellipse. Its connection with the spherical coordinates is given by $\psi = \pm\theta$ for $\phi = \pm\pi/2$.In this case, the symmetry (24) is the twofold symmetry $w(\psi) = w(\psi + \pi)$,while the symmetry (25) gives $w(\psi, -\varepsilon) = w(\pi - \psi, \varepsilon) = w(-\psi, \varepsilon)$. For linear polarization, it is $w(\psi) = w(-\psi)$.

The above symmetry relations are exact. For the direct electrons, we have the additional symmetries [39]

$$w^{(0)}(\mathbf{p}, \varepsilon) = w^{(0)}(p_x, -p_y, p_z, \varepsilon) = w^{(0)}(p_x, p_y, -p_z, \varepsilon) \quad (26)$$

and

$$w^{(0)}(\mathbf{p}, \varepsilon) = w^{(0)}(\mathbf{p}, -\varepsilon). \quad (27)$$

The relations (26) lead to the fourfold symmetry $w(\psi) = w(\pi - \psi) = w(-\psi)$, while the relation (27) has the consequence that the elliptic dichroism parameter

$$\delta(\varepsilon) \equiv \frac{w(\varepsilon) - w(-\varepsilon)}{w(\varepsilon) + w(-\varepsilon)} \quad (28)$$

is zero in the KFR approximation, $\delta^{(0)}(\varepsilon) = 0$.

Due to the symmetry relations (24) and (25), we have $w(\psi) = w(\psi + \pi)$ and $w(\psi, \varepsilon) - w(\psi, -\varepsilon) = w(\pi - \psi, -\varepsilon) - w(\pi - \psi, \varepsilon)$, so that it is enough to analyze the dichroic effects for $\psi \in [0, \pi/2]$. It is useful to introduce the angle-integrated elliptic dichroism parameter $\Delta(\varepsilon)$ by the relation

$$\Delta(\varepsilon) \equiv \frac{|W(\varepsilon) - W(-\varepsilon)|}{W(\varepsilon) + W(-\varepsilon)}, \quad (29)$$

with $W(\varepsilon) = \int_0^{\pi/2} w(\varepsilon, \psi) d\psi$.

## IV. NUMERICAL RESULTS

### A. Focal averaging

For fixed laser intensity $I$, the energy spectrum consists of a series of discrete peaks at energies $E_\mathbf{p} = E_i + n\omega - I/(4\omega^2)$, $n = n_{\min}, n_{\min}+1, \ldots$. For a detailed comparison with experimental data, this spectrum has to be integrated over the spatio-temporal intensity distribution in the laser focus. We will apply here Gaussian focal averaging as explained in Ref. [40]. For the case of weak focusing (as is the case in the experiment [4]), the diameter of the atomic beam is small compared with the Rayleigh range of the laser beam focus, and the focal-averaged electron yield is

$$\langle w_{\mathbf{p}i} \rangle \propto \int_0^{I_{\max}} \frac{dI}{I} \left( \ln \frac{I_{\max}}{I} \right)^{1/2} \sum_n w_{\mathbf{p}i}(n) \delta(E_\mathbf{p} - E_i - n\omega + I/(4\omega^2)), \quad (30)$$

where $I_{\max}$ is the peak intensity. The $\delta$ function cancels the integral over $I$ so that, for every $\mathbf{p}$, $\langle w_{\mathbf{p}i} \rangle$ can be calculated as a single sum over $n \geqslant (E_\mathbf{p} - E_i)/\omega$.

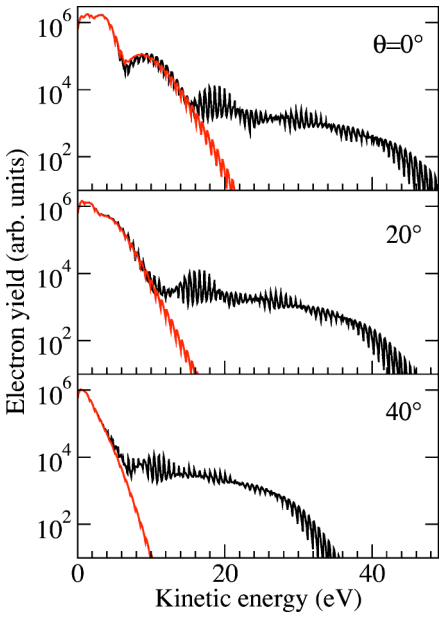


FIG. 1. (Color online) The focal averaged electron spectrum for $F^-$ ($E_i = -3.4$ eV) for a laser wavelength of 1800 nm and peak intensity $I_{\max} = 1.5 \times 10^{13}$ W/cm$^2$ for three different directions with respect to the polarization axis of the linearly polarized field: $\theta = 0°$, 20°, and 40°. The direct detachment spectra are presented by gray (red) curves, while the black curves also include detachment with rescattering.

In Figs. 1 and 2 we show examples of the spectra for

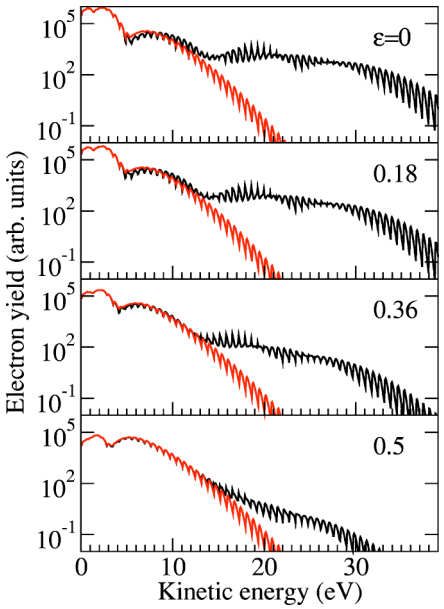


FIG. 2. (Color online) The focal-averaged electron spectrum for $F^-$ in the direction of the major polarization axis for four different ellipticities: $\varepsilon = 0$, 0.18, 0.36, and 0.5. The laser wavelength is 1800 nm and the peak intensity is $I_{\max} = 10^{13}$ W/cm$^2$. The direct detachment spectra are presented by gray (red) curves, while the black curves also include detachment with rescattering.

different angles and ellipticities. The spectrum is averaged over the spatio-temporal intensity distribution in the laser focus that corresponds to the experiment [4]. The finite momentum resolution of the detector is not taken into account. According to Ref. [3], it amounts to $\Delta E < 1$ eV for $E_{\mathbf{p}} \lesssim 15$ eV, so that it suppresses the peaks and makes them smoother. Except for the lowest energies, the calculated focal-averaged spectra display well-resolved peaks. At low energies, the spectra are governed by the direct electrons. At some rather well defined higher energy, the rescattered electrons take over and form the characteristic plateau. The cutoff of the spectrum is shifted to lower values with the increase of the angle $\theta$ and/or ellipticity $\varepsilon$. The noticeable feature of the rescattered spectra is pronounced enhancements. These enhancements are also very pronounced in experimental ATI spectra, see [22]. For theoretical developments, see Ref. [23]. The plateau in the spectrum of the low-energy direct electrons disappears with the increase of the angle $\theta$, while for the high-energy rescattered electrons only the cutoff position of the plateau is shifted to lower values. In contrast, the rescattered plateau disappears with the increase of the ellipticity, while the direct plateau is less affected.

A comparison of the experimental data from Ref. [4] (only electrons with $E_{\mathbf{p}} < 18$ eV were registered) and the theoretical results for $\theta = 0$ and $\varepsilon = 0$ were presented in our earlier paper [29] and in Ref. [34]. Both papers found better agreement for a peak intensity higher than reported in [4]. A qualitative discrepancy between the theory and the data that could not be removed by adjusting the intensity was observed in the region near 15 eV. We conjectured [29] that this discrepancy might be due to many-electron contributions to ATD that are beyond the single-active-electron approximation, as in one-photon photodetachment [41]. Indeed, Ref. [34] attributes the peaks near 15 eV to the shape resonance, which in $F^-$ is located at 14.85 eV (see p. 611 in Ref. [42]).

### B. Dependence on the initial state

In order to analyze general properties of the detachment rates, in Figs. 3 and 4 we present results obtained without focal averaging. The detachment rates by a linearly polarized field are plotted as functions of the electron energy in units of the ponderomotive energy for different emission directions and for $H^-$ (Fig. 3) and $F^-$ (Fig. 4). The figures show that the ultimate high-energy cutoff of the spectrum depends on the angle $\theta$ and is the same for both $H^-$ and $F^-$. It is at $10U_P$ for $\theta = 0$ and decreases with increasing $\theta$. The low-energy part of the spectrum is determined by the direct detachment rates. One can notice that the direct part appears to have different cutoffs for $H^-$ and $F^-$: while the rates for $H^-$ quickly decrease for energies above $2U_P$, the direct rates for $F^-$ extend to higher energies and start to decrease noticably only above the higher energy $3U_P$.

In order better to understand the behavior of the direct detachment rates, we recall that they can be obtained from Eqs. (14)–(17) solving the integral over $\varphi = \omega t$ using the saddle-point method [see Eq. (22)]. For fixed electron momentum $\mathbf{p}$, for a linearly polarized laser field there are two

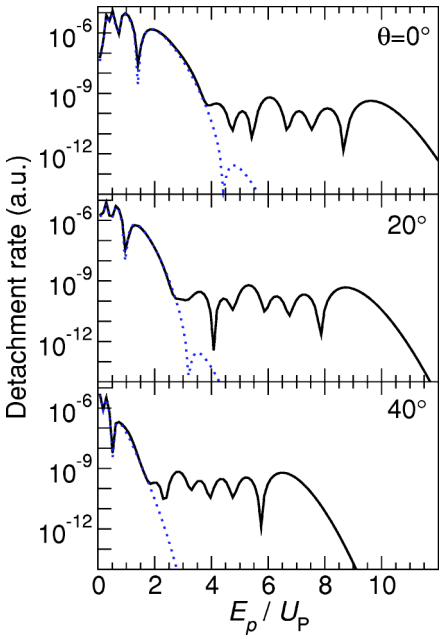


FIG. 3. Detachment rates of $H^-$ ($E_i = -0.75$ eV) as functions of the electron energy $E_{\mathbf{p}}$ (scaled to the ponderomotive energy $U_P$) for different angles: $\theta = 0°$ (upper panel), 20° (middle panel), and 40° (bottom panel). The laser-field intensity is $I = 10^{11}$ W/cm$^2$ and the wavelength is $\lambda = 10\,600$ nm. The dotted lines correspond to direct detachment.

solutions of the saddle-point equation $q^2 + \kappa^2 = 0$ (see Appendix E) so that

$$T^{(0)}_{\mathbf{p}i}(n) \propto M_1 + (-1)^l M_2, \quad M_s = \frac{\exp(iS_s)}{\sqrt{-S_s''}}. \tag{31}$$

For example, for the detachment of electrons in the direction of a linearly polarized field, we have $S = n\varphi + (pA_L$

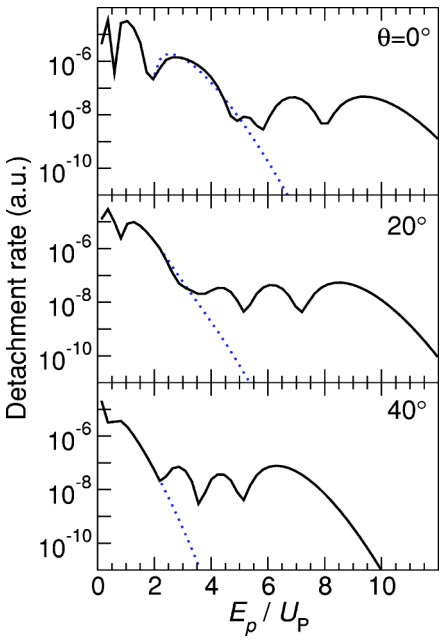


FIG. 4. Same as Fig. 3, but for $F^-$, $I = 10^{13}$ W/cm$^2$, $\lambda = 1800$ nm.

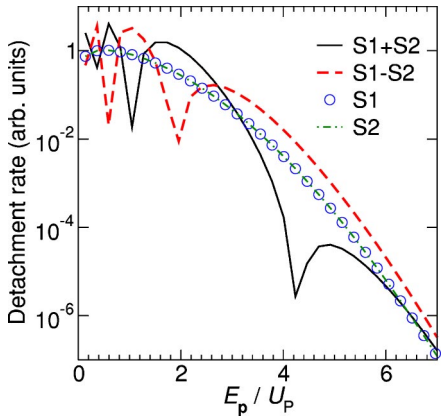


FIG. 5. (Color online) Electron spectrum in the direction $\theta=0°$ for direct ATD of $F^-$ by a linearly polarized laser with a wavelength of 1800 nm and intensity $10^{13}$ Wcm$^{-2}$. The results are obtained taking only one of the two saddle-point solutions (dot-dashed curve and circles) or taking both solutions but with different ground state: a fictitious $l=0$ ground state (solid curve "S1+S2") and the correct $l=1$ ground state (dashed curve "S1−S2"). Notice that the positions of destructive and constructive interference are almost (at least for low energies) complementary for $l=0$ and $l=1$.

$+U_P \cos\varphi)\sin\varphi/\omega$, $-S''=(p+A_L\cos\varphi)E_L\sin\varphi$, $\varphi_1=\arccos[(-p-i\kappa)/A_L]$, $\varphi_2=2\pi-\varphi_1^*$, $\mathrm{Im}\,\varphi\geqslant 0$, $0\leqslant \mathrm{Re}\,\varphi<2\pi$. In Fig. 5, we compare the rates obtained taking only solution 1 (circles), only solution 2 (dot-dashed curve), both solutions with $l=0$ (solid curve denoted by "S1+S2"), and both solutions with $l=1$ (dashed curve denoted by " S1−S2"). We see that the contributions of the solutions 1 and 2 are practically identical. Near $4.2U_P$ they interfere destructively for $l=0$, while they interfere constructively for $l=1$. These results are in agreement with numerical results presented in [29] and Eq. (1) of Ref. [4]. The very pronounced difference between the complete spectra for $l=0$ and $l=1$ is due to the different behavior of the *direct* electrons. Owing to the destructive interference near $E_\mathbf{p}\approx 4.2U_P$ for $l=0$, the direct electrons appear to have their cutoff at lower energies for $l=0$ than for $l=1$. Therefore, for $l=0$ the rescattered electrons have a chance to become dominant for lower electron energies than for $l=1$.

For increasing ellipticity, the saddle-point equation (21) keeps having two solutions per cycle up to a certain "critical" ellipticity $\varepsilon_{cr}=0.755$ [43]. For $\varepsilon>\varepsilon_{cr}$, there is only one solution per cycle, and the interferences considered above cease to exist. For circular polarization ($\varepsilon=\pm 1$), this solution is given by $\cos(\varphi-\rho)=-(\mathbf{p}^2+2U_P+\kappa^2)/\sqrt{2U_P(p_y^2+p_z^2)}$, $\tan\rho=\varepsilon p_y/p_z$. The absence of interferences for circular polarization has been confirmed by the most recent ATD experiment [44].

### C. Analogy with double-slit diffraction

For a linearly polarized laser field, the saddle-point equation (21) for specified $\mathbf{p}$ has two solutions during one cycle of the field. We decompose the momentum in components parallel and perpendicular to the laser field, $\mathbf{p}=(p_\parallel,\mathbf{p}_\perp)$, and refer to the two solutions by $t_1$ and $t_2$ ($\mathrm{Re}\,t_1<\mathrm{Re}\,t_2$). They satisfy

$$[p_\parallel + A(t_i)]^2 = 2E_i - \mathbf{p}_\perp^2 \quad (i=1,2). \tag{32}$$

Let us ignore, for sufficiently high intensity, the right-hand side of this equation so that $t_1$ and $t_2$ are real [provided $|p_\parallel|\leqslant \max|A(t)|$]. After its birth at either one of these two times, the electron then follows the classical orbits

$$\mathbf{v}_i(t)=\mathbf{p}+\mathbf{A}(t), \quad \mathbf{p}=(p_\parallel,\mathbf{p}_\perp)=(-A(t_i),\mathbf{p}_\perp),$$

$$\mathbf{x}_i(t)=(t-t_i)\mathbf{p}+\int_{t_i}^{t} d\tau\mathbf{A}(\tau). \tag{33}$$

When an electron is born at the time $t_2$, an electron born at the earlier time $t_1$ would have reached the turning point of its motion, which is at the distance

$$\mathbf{x}_1(t_2)=(t_2-t_1)\mathbf{p}+\int_{t_1}^{t_2} d\tau\mathbf{A}(\tau)\equiv\Delta\mathbf{x} \tag{34}$$

from its starting point at the origin at the position of the ion. The subsequent motion of these two electrons is identical, except that one is delayed with respect to the other by the distance $\Delta\mathbf{x}$. Hence, there are two different points of view: electronic wave packets originate at the same position—the position of the ion—at different times, or at the same time but at different positions—at the ion and at the turning point of the ponderomotive motion. Both are equivalent.

The direct quantum-mechanical transition amplitude (22) incorporates the superposition of these two orbits. It can be written in the form

$$T_{\mathbf{p}i}^{(0)}(n)=Ce^{iS_{\mathbf{p}i}(t_1)}\{1+(-1)^l e^{i[S_{\mathbf{p}i}(t_2)-S_{\mathbf{p}i}(t_1)]}\}, \tag{35}$$

where the prefactor $C$ combines the square root and the form factor on the right-hand side of Eq. (22). [The factor of $(-1)^l$ that multiplies the second term comes from the parity of the ground state in Eq. (22) and the fact that $\mathbf{E}(t_2)=-\mathbf{E}(t_1)$, while $p+A_L\cos\omega t_{2,1}=\pm i\kappa$.] Let us consider the case where $|\mathbf{p}|\ll\max|A_0(t)|$, so that we may neglect the first contribution to $\Delta\mathbf{x}$ with respect to the second. Moreover, for small $|\mathbf{p}|$, the electrons are born near the maxima of the field so that $t_2-t_1\approx T/2$ and

$$S_{\mathbf{p}i}(t_2)-S_{\mathbf{p}i}(t_1)=(\mathbf{p}^2/2+U_P-E_i)T/2+\mathbf{p}\cdot\Delta\mathbf{x}. \tag{36}$$

But, for a not too short pulse, we have

$$\mathbf{p}^2/2+U_P-E_i\approx n\omega \tag{37}$$

for some integer $n$. Hence, we obtain the interference pattern of a two-slit source,

$$\left|1+(-1)^l e^{i[S_{\mathbf{p}i}(t_2)-S_{\mathbf{p}i}(t_1)]}\right|^2=2[1+(-1)^{n+l}\cos(\mathbf{p}\cdot\Delta\mathbf{x})]. \tag{38}$$

This is a rederivation of a result by Gribakin and Kuchiev [24]; see also [25,26]. For simplicity, we have treated $\Delta\mathbf{x}$ as real, which restricts us to the tunneling limit.

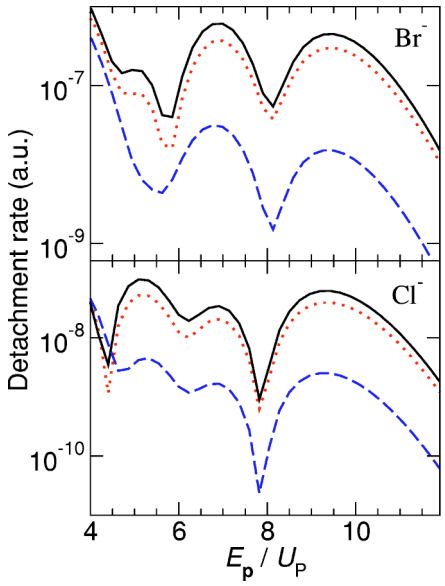


FIG. 6. (Color online) ATD electron spectra (solid curves) for $Br^-$ (upper panel) and $Cl^-$ (lower panel) in the direction of the laser polarization. The contributions of the polarization part (C4) (dashed curves) and the static part (C8) (dotted curves) of the rescattering potential are analyzed.

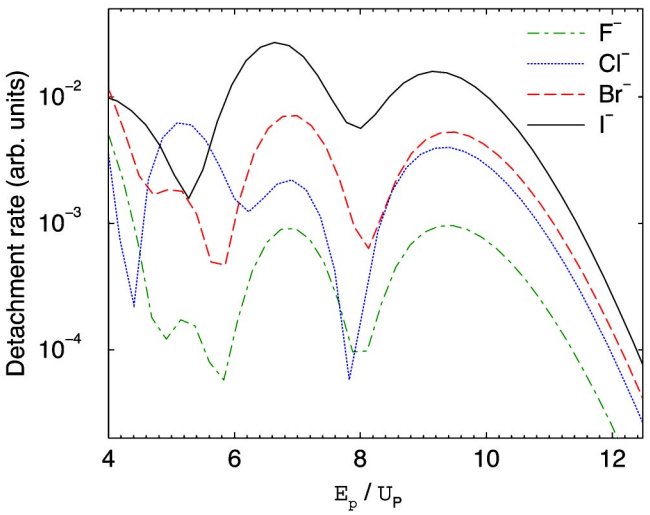


FIG. 7. (Color online) ATD electron spectra normalized so that the maximum of their direct low-energy part is equal to 1. Only the high-energy part with $E_p > 4U_P$ is shown. The laser intensity is $10^{13}$ W/cm$^2$, the wavelength 1800 nm, and $\theta = 0$. The laser field is linearly polarized and no focal averaging is taken. The spectra are for $F^-$ (dot-dashed line), $Cl^-$ (dotted line), $Br^-$ (dashed line), and $I^-$ (solid line), with the relevant parameters given in the Appendixes.

### D. Dependence on the rescattering potential

In our previous paper [29], we have analyzed the influence of the static and polarization potentials on the high-energy ATD spectra. The examples of $H^-$ and $F^-$ ions were investigated (please notice that the laser intensity for $F^-$ was $1.1 \times 10^{13}$ W/cm$^2$ and not $10^{13}$ W/cm$^2$ as mentioned in Fig. 4 of Ref. [29]). We also noticed that for $H^-$, the polarization potential makes a slightly stronger contribution than the static potential, while for $F^-$ the contribution of the static potential is dominant. Here we will analyze the spectra of heavier halogen ions. In Fig. 6, we present high-energy ($E_p > 4U_P$) ATD spectra for $Br^-$ and $Cl^-$. The laser intensity and wavelength are $10^{13}$ W/cm$^2$ and 1800 nm, respectively. We see that both for $Cl^-$ (lower panel) and $Br^-$ (upper panel), the total spectrum (solid lines) is mainly determined by the contribution of the static rescattering potential (C8) (dotted

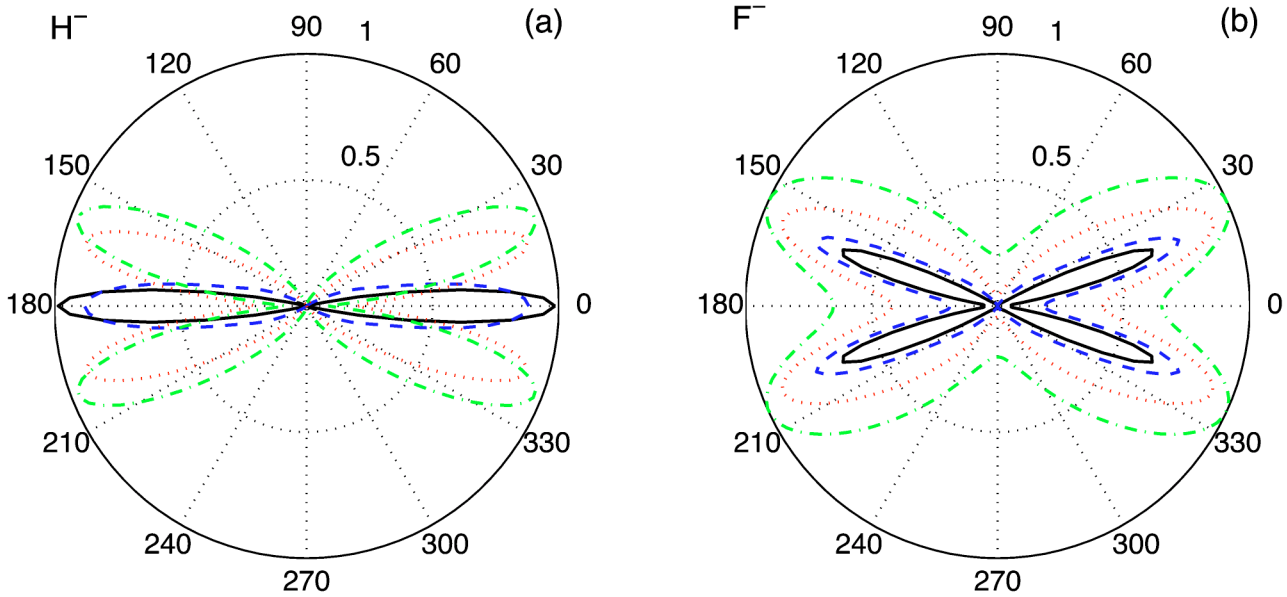


FIG. 8. (Color online) Detachment rates, Eq. (C11) as functions of the polar angle $\psi$, $\tan\psi = p_y/p_z$ (see Sec. III), for fixed electron energy $E_p = 2U_P$, for different ellipticities: $\varepsilon = 0$ (solid black line), $\varepsilon = 0.18$ (dashed blue line), $\varepsilon = 0.36$ (dotted red line), and $\varepsilon = 0.5$ (dot-dashed green line), and for (a) $H^-$, laser intensity $10^{11}$ W/cm$^2$ and wavelength 10 600 nm, rates in $x \times 10^{-7}$ a.u., with $x = 2.25$ for $\varepsilon = 0$, $x = 1.6$ for $\varepsilon = 0.18$, and $x = 0.8$ for $\varepsilon = 0.36$ and 0.5; (b) $F^-$, intensity $10^{13}$ W/cm$^2$ and wavelength 1800 nm, rates in $5.25 \times 10^{-7}$ a.u.

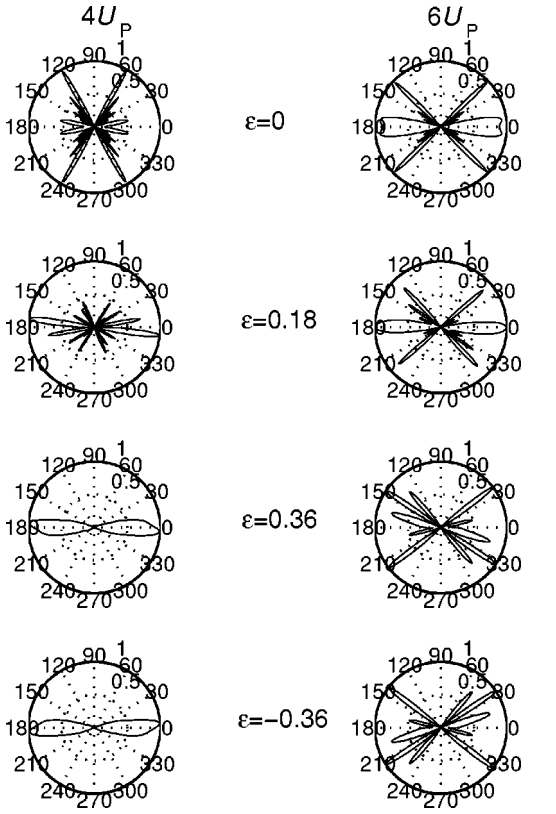


FIG. 9. Polar diagrams of the high-energy detachment rates of $H^-$ for the same laser parameters as in Fig. 8(a), for $E_{\mathbf{p}}=4U_{\mathrm{P}}$ (left-hand panels), $E_{\mathbf{p}}=6U_{\mathrm{P}}$ (right-hand panels), and for the ellipticity $\varepsilon=0$ (top panels), $\varepsilon=0.18$ (panels in the second row), $\varepsilon=0.36$ (third row), and $\varepsilon=-0.36$ (bottom row). The rates for $E_{\mathbf{p}}=4U_{\mathrm{P}}$ (left-hand panels) are in multiples of $x\times10^{-10}$ a.u., with $x=1.5$, 0.9, and 1.07 for $\varepsilon=0$, 0.18, and $\pm0.36$, respectively. For $E_{\mathbf{p}}=6U_{\mathrm{P}}$ (right-hand panels) we have $x=1.1$, 0.33, and 0.004 38 for $\varepsilon=0$, 0.18, and $\pm0.36$, respectively.

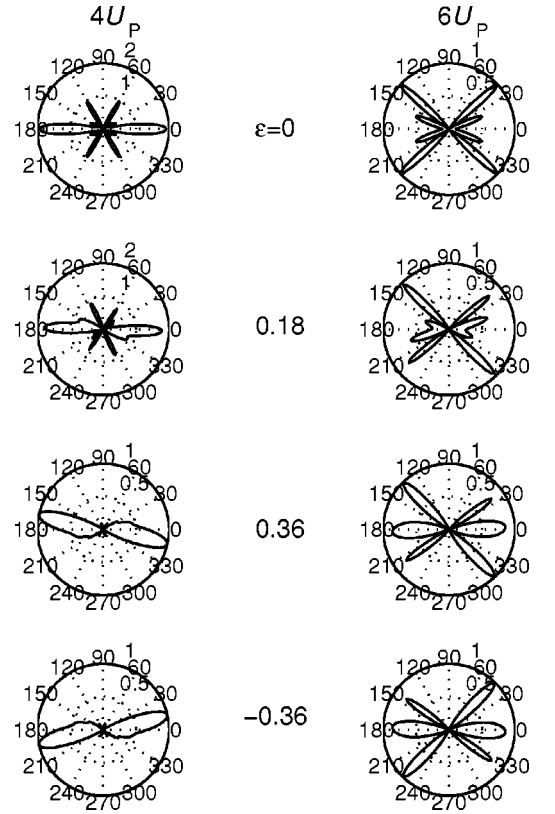


FIG. 10. The same as in Fig. 9 but for $F^-$ and for the laser parameters of Fig. 8(b). The rates for $E_{\mathbf{p}}=4U_{\mathrm{P}}$ (left-hand panels) are in multiples of $1.25\times10^{-8}$ a.u., except for $\varepsilon=0$, for which they are in multiples of $2\times10^{-8}$ a.u. For $E_{\mathbf{p}}=6U_{\mathrm{P}}$ (right-hand panels) they are in $x\times10^{-9}$ a.u., with $x=13.2$ for $\varepsilon=0$, $x=7.9$ for $\varepsilon=0.18$, and $x=0.87$ for $\varepsilon=\pm0.36$.

lines) and that the contribution of the polarization potential (C4) (dashed lines) is small.

For $H^-$, the low-energy direct detachment rates are almost five orders of magnitude larger than those of the rescattering plateau. For the heavier halogen ions, the static part of the rescattering potential is much stronger so that the rescattering plateau becomes higher. In order to explore this, in Fig. 7 we compare the rescattering parts of the negative-halogen-ion spectra. The spectra are normalized so that the maxima of their direct parts are equal to 1. In this way, we are able to compare the relative heights of the rescattering plateaus for $F^-$, $Cl^-$, $Br^-$, and $I^-$. As expected, because the number of scattering centers is the largest for iodine, the corresponding plateau is the highest. It is lower than the direct part of the spectrum by a factor only 40. The heights of the rescattering plateaus decrease from iodine to fluorine by a factor of about 30, but even the plateau in fluorine is still higher than the one in $H^-$ by almost two orders of magnitude. Therefore, the heavier negative halogen ions are excellent candidates for an experimental observation of the rescattering plateau.

### E. Elliptical polarization

First, we will present numerical results for the low-energy electrons. According to the symmetry considerations of Sec. III, the detachment rates should obey the fourfold symmetry (26) which holds regardless of the angular momentum of the ground state. This is confirmed by Fig. 8, which displays $w\psi$ polar diagrams for $E_{\mathbf{p}}=2U_{\mathrm{P}}$, for various ellipticities, and for $H^-$ ($l=0$) and $F^-$ ($l=1$) ions.

Next, in Figs. 9 and 10 we show results for the higher energies $E_{\mathbf{p}}=4U_{\mathrm{P}}$ and $6U_{\mathrm{P}}$. For $\varepsilon=0$, the fourfold symmetry is preserved, as it should, and the spectrum shows the typical sidelobes (see Ref. [12] and references therein). For nonzero ellipticity, the fourfold symmetry is violated but the twofold symmetry (24) is preserved. Comparing the results for $\varepsilon=0.36$, with those for $\varepsilon=-0.36$, we confirm that the symmetry relation (25) is satisfied.

Finally, in Fig. 11 the angle-integrated elliptic dichroism parameter $\Delta(\varepsilon)$, defined in Eq. (29), is shown for $F^-$ ions as a function of ellipticity for various electron energies. For energies less than $3U_{\mathrm{P}}$, this parameter is close to zero because this part of the spectrum is dominated by the direct electrons for which $\Delta^{(0)}(\varepsilon)=0$ in view of Eq. (27). For higher energies, $\Delta(\varepsilon)$ is a smooth function of $\varepsilon$. It assumes its maxi-

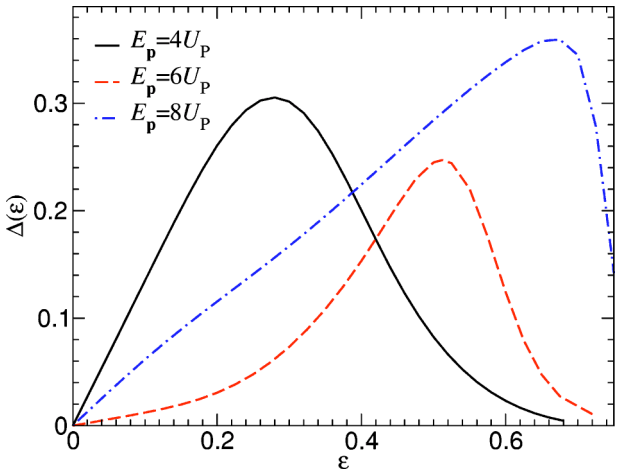


FIG. 11. (Color online) Angle-integrated elliptic dichroism parameter as a function of the ellipticity for $F^-$, laser intensity $10^{13}$ W/cm$^2$, and wavelength 1800 nm. The detached electron energy is $E_p=4U_P$ (solid curve), $E_p=6U_P$ (dashed curve), and $E_p=8U_P$ (dot-dashed curve).

mum of $\Delta(\varepsilon=0.28)=0.31$ for $E_p=4U_P$, $\Delta(\varepsilon=0.51)=0.25$ for $E_p=6U_P$, while for $E_p=8U_P$ the maximum is $\Delta(\varepsilon=0.67)=0.36$. Ultimately, when the ellipticity approaches circular polarization, elliptic dichroism disappears. Maybe surprisingly, Fig. 11 shows that, for lower electron energies, this tendency already develops for rather low ellipticity.

## V. CONCLUSIONS

The energy spectra of electrons detached from negative ions are characterized by two regions. The low-energy region (below $2-4\ U_P$, depending on the parity of the ground state) is dominated by the direct electrons and is strongly affected by the parity of the ground state. The spectrum is made up by two contributions, which can be attributed to electrons entering the continuum at different times during the field cycle. The parity dependence is particularly important in the region around $3-4U_P$ where these two contributions interfere constructively for odd parity and destructively for even parity. This is relevant to the interpretation of the experiment with $F^-$ ($l=1$) [4]. The apparent plateau in the region in question is caused by this constructive interference.

The high-energy spectral region is characterized by the rescattering plateau whose yield is below that of the direct electrons by several orders of magnitude, depending on the ionic species. Its start depends upon how quickly the yield of the direct electrons drops with increasing energy, as just discussed. Hence, for $H^-$ it starts between 2 and 3 $U_P$, while for $F^-$ its onset is at significantly higher energies above $4U_P$. In any case, for a linearly polarized field and electrons emitted in the direction of the field, it starts rolling off near its classical cutoff at $10U_P$. The shape of this plateau is determined by the laser field parameters, in particular the ellipticity, and on the direction of electron emission, but it is essentially independent of the angular momentum of the ionic ground state. However, its height strongly depends on the number of rescattering centers. This number is higher for the heavier negative halogen ions so that these are excellent candidates for an experimental detection of the rescattering plateau for negative ions.

The angular distribution of high-energy electrons is strongly affected by the laser ellipticity. A measure of the asymmetry introduced by the ellipticity is the angle-integrated elliptic dichroism parameter introduced in this paper.

For elliptical polarization, there are only few experimental data for high-order ATI of atoms [45,46] and none for high-order ATD of ions. For rare-gas atoms and the pertinent laser parameters, theoretical calculations based on the same formalism discussed in this paper and interpreted in terms of quantum orbits can be found in Refs. [45,47]. They show features very similar to Figs. 9 and 10, in particular the lack of symmetry with respect to the two polarization axes. In view of the lingering doubts regarding the significance of Coulomb effects even for high-order ATI, experiments with negative ions, where the absence of the long-range Coulomb potential facilitates the comparison of theory and experiments, are highly desirable.

## ACKNOWLEDGMENTS

We enjoyed discussions with M. V. Frolov, I. Yu. Kiyan, N. L. Manakov, G. G. Paulus, H. Rottke, and A. F. Starace. This work was supported in part by VolkswagenStiftung and by the Federal Ministry of Education and Science, Bosnia and Herzegovina.

## APPENDIX A: INTEGRAL OVER THE INTERMEDIATE ELECTRON MOMENTA

In Eq. (9), having inserted the expansion (6) of the Volkov time-evolution operator, we are concerned with an integral of the type

$$I(\alpha,\mathbf{k}_s)=\int d^3\mathbf{k} f(\mathbf{k})\exp[i\alpha(\mathbf{k}-\mathbf{k}_s)^2]. \tag{A1}$$

Shifting repeatedly the integration variable $\mathbf{k}$, we may write

$$\begin{aligned} I(\alpha,\mathbf{k}_s) &= \int d^3\mathbf{k} f(\mathbf{k}+\mathbf{k}_s)\exp(i\alpha\mathbf{k}^2) \\ &= \int d^3\mathbf{k}\ \exp(\mathbf{k}\cdot\partial/\partial\mathbf{k}_s) f(\mathbf{k}_s)\exp(i\alpha\mathbf{k}^2) \\ &= \int d^3\mathbf{k}\ \exp\left[i\alpha\left(\mathbf{k}+\frac{1}{2i\alpha}\frac{\partial}{\partial\mathbf{k}_s}\right)^2\right]\exp\left(\frac{i}{4\alpha}\frac{\partial^2}{\partial\mathbf{k}_s^2}\right) f(\mathbf{k}_s) \\ &= \left(\frac{i\pi}{\alpha}\right)^{3/2}\exp\left(\frac{i}{4\alpha}\frac{\partial^2}{\partial\mathbf{k}_s^2}\right) f(\mathbf{k}_s), \end{aligned} \tag{A2}$$

which is a formal solution of the integral. This yields Eq. (11) of the main body of the paper.

The three-dimensional integral over the intermediate electron momenta (A1) appears frequently in consideration of higher-order atomic processes in strong fields. The exact solution of this integral was presented in the form of a power series in Ref. [48] in the context of high-order harmonic

generation. Later on it was used for high-order above-threshold ionization [12], laser-assisted x-ray–atom scattering [18], and electron-ion recombination [19]. In the special cases when the atomic system is modeled by the zero-range potential [31,49], this integral can be solved exactly (only the zeroth-order term of the mentioned power series survives [50]). An exact solution also exists for a Gaussian potential (see [51] and references therein). In this appendix, we have considered the solution of this integral in the context of the rescattering matrix element $M_{\mathbf{p}i}^{(1)}$.

## APPENDIX B: MATRIX ELEMENTS FOR DIRECT ATD

The amplitude of direct ATD can be obtained by calculating the integral over time $t$, i.e., over the variable $\varphi=\omega t$. This can also be done by using the saddle-point method as in [24]. We will prefer here the numerical integration. The ground-state wave functions of the negative ion in momentum space, which appear as the subintegral functions, are given in [24]. We will present here explicit expressions for the negative halogen ions we are interested in. According to Ref. [24], we have

$$\psi_i \equiv \psi_{lm}(\mathbf{r}) = (A/r)\exp(-\kappa r)Y_{lm}(\hat{\mathbf{r}}), \tag{B1}$$

where $E_i=-\kappa^2/2$ and for

$$\mathrm{H}^-: \quad l=0, \quad A=0.75, \quad \kappa=0.235, \tag{B2}$$

$$\mathrm{F}^-: \quad l=1, \quad A=0.7, \quad \kappa_{3/2}=0.4998, \quad \kappa_{1/2}=0.5035, \tag{B3}$$

while according to [52] we have

$$\mathrm{Cl}^-: \quad A=1.34, \quad \kappa=0.516,$$

$$\mathrm{Br}^-: \quad A=1.49, \quad \kappa=0.498,$$

$$\mathrm{I}^-: \quad A=1.9, \quad \kappa=0.475, \tag{B4}$$

with $l=1$ and $j=3/2$. In our paper, the calculations for $\mathrm{F}^-$ were done for $j=1/2$. Using Eq. (19), we get

$$\tilde{\psi}_{00}(\mathbf{q}) = \frac{4\pi A}{(2\pi)^{3/2}}\frac{Y_{00}(\hat{\mathbf{q}})}{q^2+\kappa^2}, \tag{B5}$$

$$\tilde{\psi}_{1m}(\mathbf{q}) = i\frac{4\pi A}{(2\pi)^{3/2}}qf(q)Y_{1m}(\hat{\mathbf{q}}), \tag{B6}$$

where

$$f(q) = \frac{1}{q^2}\left(\frac{\kappa}{q^2+\kappa^2}-\frac{1}{q}\arctan\frac{q}{\kappa}\right) = -\frac{2}{\kappa^3}\sum_{n=0}^{\infty}(-1)^n\frac{n+1}{2n+3}\left(\frac{q}{\kappa}\right)^{2n}. \tag{B7}$$

According to Eq. (17) and with the explicit expressions for the spherical harmonics $Y_{lm}$, the direct amplitudes $\mathcal{T}_{\mathbf{p}i}^{(0)}$ are

$$\mathcal{T}_{\mathbf{p}00}^{(0)} = -\frac{A}{\sqrt{8\pi^2}}, \tag{B8}$$

$$\mathcal{T}_{\mathbf{p}1m}^{(0)} = -\frac{iA\sqrt{6}}{4\pi}(q^2+\kappa^2)qf(q)s(\theta_q,\phi_q), \tag{B9}$$

with

$$s(\theta_q,\phi_q) = \delta_{m,0}\cos\theta_q - \frac{m}{\sqrt{2}}\sin\theta_q e^{im\phi_q}. \tag{B10}$$

For the detached electron momentum $\mathbf{p}=(p,\theta,\phi)$ and $q=|\mathbf{p}+\mathbf{A}(\varphi)|$, the angles $\theta_q$ and $\phi_q$ are determined by the expressions

$$q\cos\theta_q = p\cos\theta + \frac{E_\mathrm{L}\cos\varphi}{\omega\sqrt{1+\varepsilon^2}},$$

$$\sin\theta_q = \sqrt{1-\cos^2\theta_q},$$

$$q\sin\theta_q\cos\phi_q = p\sin\theta\cos\phi,$$

$$q\sin\theta_q\sin\phi_q = p\sin\theta\sin\phi + \frac{\varepsilon E_\mathrm{L}\sin\varphi}{\omega\sqrt{1+\varepsilon^2}}, \tag{B11}$$

for the elliptically polarized laser field (23). For a linearly polarized field along the $z$ axis, we have $\phi_q=\phi$.

An alternative form of the matrix element $T_{\mathbf{p}lm}^{(0)}$ can be obtained using Eq. (8) and the first equation in Eq. (17). The result is

$$\mathcal{T}_{\mathbf{p}00}^{(0)} = -i\frac{A\sqrt{2}}{\pi}\frac{\mathbf{E}(\varphi)\cdot\mathbf{q}}{(q^2+\kappa^2)^2}, \tag{B12}$$

and, for linear polarization,

$$\mathcal{T}_{\mathbf{p}1m}^{(0)} = \frac{A\sqrt{6}}{2\pi}E_\mathrm{L}\sin\varphi\left[\delta_{m,0}h + \sin\theta_q\frac{\partial s}{\partial\theta_q}(h+f)\right], \tag{B13}$$

with

$$h(q) = -\left(1+\frac{\partial}{\partial q}\right)f(q) = \frac{2\kappa(2q^2+\kappa^2)}{q^2(q^2+\kappa^2)^2} - \frac{2}{q^3}\arctan\frac{q}{\kappa} = \frac{2}{\kappa^3}\sum_{n=0}^{\infty}(-1)^n\frac{(n+1)(2n+1)}{2n+3}\left(\frac{q}{\kappa}\right)^{2n}. \tag{B14}$$

For linear polarization, the dependence on $\phi_q=\phi$ in Eq. (B10) disappears after taking the absolute square of $\exp(im\phi)$ in the detachment rate. For elliptical polarization, the matrix element (B13) has the more complicated form

$$\mathcal{T}_{\mathbf{p}1m}^{(0)} = -\sqrt{\frac{3}{2^{|m|+1}}}\frac{A}{\pi}\frac{E_\mathrm{L}e^{im\phi}}{\sqrt{1+\varepsilon^2}}\{(h+f)\sin\theta_q[\sin\theta_q'\sin\varphi + \varepsilon\cos\theta_q'\sin\phi_q\cos\varphi] + i|m|f\varepsilon e^{-im\phi}\cos\varphi + (|m|-1)h\sin\varphi\}, \tag{B15}$$

with $\theta_q'=\theta_q+m\pi/2$.This form of the matrix element we will also need in Appendix C.

## APPENDIX C: MATRIX ELEMENTS FOR ATD WITH RESCATTERING

According to Eq. (18), in order to calculate the rescattered electron spectrum, we need the matrix element

$$\langle \mathbf{g}|\mathbf{r}|\psi_i\rangle = i\frac{\partial}{\partial \mathbf{g}}\tilde{\psi}_i(\mathbf{g}), \tag{C1}$$

where the vector $\mathbf{g}=\mathbf{k}_s+\mathbf{A}(\varphi-\omega\tau)$ [see Eq. (12)] lies in the laser polarization plane. Using the results of Appendix B, we get

$$\langle \mathbf{g}|\mathbf{r}|\psi_{00}\rangle = -\frac{iA\sqrt{2}}{\pi}\frac{\mathbf{g}}{(g^2+\kappa^2)^2}. \tag{C2}$$

For the elliptically polarized field, the matrix element $\langle \mathbf{g}|\mathbf{r}\cdot\mathbf{E}(\varphi)|\psi_{1m}\rangle$ is given by Eq. (B15) with $\varphi\to\varphi-\omega\tau$, $\mathbf{q}\to\mathbf{g}$, $\phi_g=\mathrm{sgn}(\mathbf{g}\cdot\hat{\mathbf{e}}_y)\pi/2$, and $\cos\theta_g=\hat{\mathbf{g}}\cdot\hat{\mathbf{e}}_z$, $\sin\theta_g=|\hat{\mathbf{g}}\cdot\hat{\mathbf{e}}_y|$. For a linearly polarized field along the $z$ axis, we have

$$\langle \mathbf{g}|\mathbf{r}\cdot\hat{\mathbf{e}}_z|\psi_{1m}\rangle = \delta_{m,0}\frac{A\sqrt{6}}{2\pi}h(g). \tag{C3}$$

We also need the Fourier transform of the rescattering potential $V$. We have $V(r)=V_S(r)+V_P(r)$, where $V_P$ is the polarization potential,

$$V_P(r) = -\frac{\alpha_P}{2(r^2+d^2)^2}, \quad d^4=\frac{\alpha_P}{2Z^{1/3}}, \tag{C4}$$

with $\alpha_P(\mathrm{H})=4.5$ a.u., $\alpha_P(\mathrm{F})=3.76$ a.u., $\alpha_P(\mathrm{Cl})=14$ a.u., $\alpha_P(\mathrm{Br})=30$ a.u., $\alpha_P(\mathrm{I})=27$ a.u., $Z(\mathrm{H})=1$, $Z(\mathrm{F})=9$, $Z(\mathrm{Cl})=17$, $Z(\mathrm{Br})=35$, and $Z(\mathrm{I})=53$. The Fourier transform of $V_P$ is

$$V_{\mathbf{K}}^{(P)} = -\frac{\alpha_P}{16\pi d}\exp(-Kd). \tag{C5}$$

The static potential $V_S$ for $H^-$ can be calculated exactly, with the result

$$V_S(r) = -\left(1+\frac{1}{r}\right)e^{-2r} \tag{C6}$$

and

$$V_{\mathbf{K}}^{(S)} = -\frac{1}{2\pi^2}\frac{K^2+8}{(K^2+4)^2}. \tag{C7}$$

The static potential for fluorine can be modeled by the double Yukawa potential,

$$V_S(r) = -\frac{Z}{H}\frac{e^{-r/D}}{r}[1+(H-1)e^{-Hr/D}], \tag{C8}$$

with $D=0.575$, $H=DZ^{0.4}$, and with the Fourier transform

$$V_{\mathbf{K}}^{(S)} = -\frac{Z}{2\pi^2 H}\left[\frac{1}{K^2+D^{-2}}+\frac{H-1}{K^2+\left(\frac{H+1}{D}\right)^2}\right]. \tag{C9}$$

The vector $\mathbf{K}$ in the above expressions is $\mathbf{K}=\mathbf{k}_s-\mathbf{p}$.

It should be mentioned that our detachment rate $w_{\mathbf{p}i}(n)$, for a linearly polarized laser field, does not depend on the angle $\phi$. Namely, in the rescattering term we have the factor $\delta_{m,0}$ [see Eq. (C3)], while for the direct term we have the factor $\exp(im\phi)$ [see Eqs. (B10) and (B11)], which disappears upon taking the absolute square in Eq. (14) . For an elliptically polarized laser field, the results do not depend on $\phi$ in the special case where the electron is emitted along the major axis ($z$ axis) of the polarization ellipse, i.e., for $\theta=0$. We usually integrate over all angles $\phi$, which gives an additional factor $2\pi$ in the differential detachment rate. The rate summed over all $m$ and over the electron spin projections, and integrated over $\phi$, is then

$$W_{p\theta,l}(n) = 2\sum_{m=-l}^{l} 2\pi w_{\mathbf{p}lm}(n). \tag{C10}$$

If the effect of fine-structure splitting is taken into account, the detachment rate for the $j=l\pm1/2$ sublevel is

$$W_{p\theta,l}^{(j)}(n) = \frac{2j+1}{2l+1}W_{p\theta,l}(n). \tag{C11}$$

For example, for $F^-$ the electron affinity $\kappa_j^2/2$ is different for $j=1/2$ and $j=3/2$ [see Eq. (B3)].

## APPENDIX D: RESCATTERING POTENTIAL

In our model, we suppose that the detached electron rescatters on the residual part of its parent atom. We will neglect exchange effects. In this case, the potential $V$ on which the electron rescatters consists of two parts, $V=V_P+V_S$. The target atom is polarized by the Coulomb field of the incident electron and this effect is usually modeled by the potential

$$V_P(r) = -\frac{\alpha_P}{2(r^2+d^2)^2}, \tag{D1}$$

where $\alpha_P$ is the electrostatic dipole polarizability of the atom whose values can be found in Ref. [52]. The parameter $d$ is connected with $\alpha_P$ and the nuclear charge $Z$ by the formula $d^4=\alpha_P/(2Z^{1/3})$ [53].

The static potential $V_S$ includes the interaction of the incoming electron with the nucleus and the atomic electron cloud. It can be written in the form [54]

$$V_S(\mathbf{r}) = -\frac{Z}{r}+\int\frac{d^3\mathbf{s}}{|\mathbf{r}-\mathbf{s}|}\rho(\mathbf{s}), \tag{D2}$$

where

$$\rho(\mathbf{s}) = \sum_{j=1}^{Z}\int\prod_{k=1,k\neq j}^{Z} d^3\mathbf{r}_k|\psi_a(\mathbf{r}_1,\ldots,\mathbf{r}_{j-1},\mathbf{s},\mathbf{r}_{j+1},\ldots,\mathbf{r}_Z)|^2 \tag{D3}$$

is the density of the atomic electrons in the state $|a\rangle$. The Fourier transform of $V_S$ can be represented in the form

$$V_{\mathbf{K}}^{(S)} = \frac{1}{2\pi^2K^2}[F(\mathbf{K})-Z], \tag{D4}$$

where $F(\mathbf{K})=\int d^3\mathbf{r}\rho(\mathbf{r})\exp(i\mathbf{K}\cdot\mathbf{r})$ is a real form factor. For an electron scattering of a hydrogen atom, we have $\rho(\mathbf{r})$

$=|\psi_{1s}(\mathbf{r})|^2=\exp(-2r)/\pi$, so that $V_S$ and $V_{\mathbf{K}}^{(S)}$ are given by Eqs. (C6) and (C7), respectively. For electron scattering off helium, the wave function can be obtained variationally, with the result $\psi(r_1,r_2)=\exp[-(r_1+r_2)/b]/(\pi b^3)$, $b=16/27$, so that $\rho(r)=2\exp(-2r/b)/(\pi b^3)$ and $F(K)=2/(1+K^2b^2/4)^2$. For more complex atoms, an analytical expression for $V_{\mathbf{K}}^{(S)}$ cannot be obtained. However, numerical calculations for electron-atom scattering can be simplified significantly by using a semiempirical core potential, i.e., by effectively treating the target as one quasielectron [55]. A relatively simple analytical potential for describing elastic scattering of electrons off atoms was proposed in Refs. [56,57]. It is based on the independent-particle model for bound states of electrons in atoms, which maintains a close relationship to the Hartree-Fock model [58]. For $F^-$, $Cl^-$, $Br^-$, and $I^-$, here we use the independent-particle-model potential (C8) represented by the double Yukawa potential [59] with the parameters $H$ and $D$ given in Ref. [58], which has the Fourier transform (C9). Potentials for negative atomic ions are given in [60,61]. For more recent developments of analytical local electron-electron interaction model potentials for atoms, see Ref. [62].

## APPENDIX E: DIRECT MATRIX ELEMENT FOR ARBITRARY *l*

Let us start from Eq. (10) . In view of the wave functions (B1), we need to calculate the spatial integral

$$I_{lm}(\mathbf{q}) \equiv \int d^3\mathbf{r} e^{-i\mathbf{q}\cdot\mathbf{r}} \frac{e^{-\kappa r}}{r} Y_{lm}(\hat{\mathbf{r}}), \tag{E1}$$

where $\mathbf{q}=\mathbf{p}+\mathbf{A}(t)$. With the help of the plane-wave expansion

$$\exp(-i\mathbf{q}\cdot\mathbf{r}) = 4\pi \sum_{l=0}^{\infty} (-i)^l j_l(qr) \sum_{m=-l}^{l} Y_{lm}(\hat{\mathbf{r}}) Y_{lm}^*(\hat{\mathbf{q}}), \tag{E2}$$

we find that

$$I_{lm}(\mathbf{q}) = 4\pi Y_{lm}(\hat{\mathbf{q}})(-i)^l X_l(q) \tag{E3}$$

with

$$X_l(q) = \int_0^{\infty} r dr \exp(-\kappa r) j_l(qr). \tag{E4}$$

The temporal part of the matrix element (10) will be carried out by saddle-point integration. As a result, the momenta $\mathbf{q}$ will satisfy

$$\mathbf{q}^2 = [\mathbf{p}+\mathbf{A}(t)]^2 = -\kappa^2, \tag{E5}$$

and, in turn, the momentum components $(q_x,q_y,q_z)$ will be complex. The plane-wave expansion (E2) can immediately be analytically continued to complex values of $q_i$, since $\exp(-i\mathbf{q}\cdot\mathbf{r})$ is an entire analytic function of the momentum components $q_i$, and, on the right-hand side, so is the product $j_l(qr)Y_{lm}^*(\hat{\mathbf{q}})$. Note that individually $j_l(qr)$ and $Y_{lm}(\hat{\mathbf{q}})$ depend on odd powers of $q$ for odd $l$ and, therefore, exhibit a branch cut in $q=\sqrt{q_x^2+q_y^2+q_z^2}$.

In view of Eqs. (10) and (E5), what we actually need after having carried out the saddle-point integration is

$$\lim_{q^2+\kappa^2\to 0} (q^2+\kappa^2) X_l(q). \tag{E6}$$

Integrating by parts and using the differential equation satisfied by the spherical Bessel functions, we find

$$(q^2+\kappa^2)X_0(q) = 1, \tag{E7}$$

while for $l\neq 0$ we get

$$\begin{aligned}(q^2+\kappa^2)X_l(q) &= l(l+1)\int_0^{\infty} dr e^{-\kappa r} j_l(qr)/r \\ &= \frac{\sqrt{\pi}}{2}\left(\frac{q}{2\kappa}\right)^l \frac{\Gamma(l+2)}{\Gamma(l+3/2)} F\left(\frac{l}{2},\frac{l+1}{2};l+\frac{3}{2};-\frac{q^2}{\kappa^2}\right) \\ &= \frac{\sqrt{\pi}\Gamma(l+2)}{2^{l+1}\Gamma\left(\frac{l+3}{2}\right)\Gamma\left(\frac{l}{2}+1\right)}\left(\frac{q}{\kappa}\right)^l = \left(\frac{q}{\kappa}\right)^l,\end{aligned} \tag{E8}$$

where, evaluating the hypergeometric function, we used that $q^2=-\kappa^2$. Putting everything together, we note that the only dependence on the angular-momentum quantum numbers occurs in the form of the solid harmonics,

$$\left(\frac{q}{\kappa}\right)^l Y_{lm}(\hat{\mathbf{q}}). \tag{E9}$$

These are homogeneous polynomials of order $l$ in the Cartesian momentum components $q_i$ $(i=x,y,z)$ and, therefore, entire analytic functions of $q_i$ for any integer $l$. Once the (complex) solutions $t_s$ of the saddle-point equation (21) are determined, the momenta $\mathbf{q}=\mathbf{p}+\mathbf{A}(t_s)$ are known. Hence, there is no branch-cut-related ambiguity in the evaluation of the solid harmonics (E9) for complex momenta. This result can be applied for arbitrary ellipticity and not only for the linearly polarized case of Ref. [24].

[1] P. Agostini, F. Fabre, G. Mainfray, G. Petite, and N. K. Rahman, Phys. Rev. Lett. **42**, 1127 (1979).
[2] H. C. Bryant, A. Mohagheghi, J. E. Stewart, J. B. Donahue, C. R. Quick, R. A. Reeder, V. Yuan, C. R. Hummer, W. W. Smith, C. Cohen, W. P. Reinhardt, and L. Overman, Phys. Rev. Lett. **58**, 2412 (1987).
[3] R. Reichle, H. Helm, and I. Yu. Kiyan, Phys. Rev. Lett. **87**, 243001 (2001).
[4] I. Yu. Kiyan and H. Helm, Phys. Rev. Lett. **90**, 183001 (2003).
[5] G. G. Paulus, W. Nicklich, H. Xu, P. Lambropoulos, and H.

Walther, Phys. Rev. Lett. **72**, 2851 (1994).
[6] M. J. Nandor, M. A. Walker, L. D. Van Woerkom, and H. G. Muller, Phys. Rev. A **60**, R1771 (1999).
[7] R. Wiehle, B. Witzel, H. Helm, and E. Cormier, Phys. Rev. A **67**, 063405 (2003).
[8] L. V. Keldysh, Zh. Eksp. Teor. Fiz. **47**, 1945 (1964); [Sov. Phys. JETP **20**, 1307 (1965)]; F. H. M. Faisal, J. Phys. B **6**, L89 (1973); H. R. Reiss, Phys. Rev. A **22**, 1786 (1980); **42**, 1476 (1990).
[9] H. R. Reiss, Phys. Rev. A **54**, R1765 (1996).
[10] P. B. Corkum, Phys. Rev. Lett. **71**, 1994 (1993).
[11] A. Lohr, M. Kleber, R. Kopold, and W. Becker, Phys. Rev. A **55**, R4003 (1997).
[12] D. B. Milošević and F. Ehlotzky, Phys. Rev. A **58**, 3124 (1998); J. Phys. B **32**, 1585 (1999).
[13] L. F. DiMauro and P. Agostini, Adv. At., Mol., Opt. Phys. **35**, 79 (1995).
[14] W. Becker, F. Grasbon, R. Kopold, D. B. Milošević, G. G. Paulus, and H. Walther, Adv. At., Mol., Opt. Phys. **48**, 35 (2002).
[15] D. B. Milošević and F. Ehlotzky, Adv. At., Mol., Opt. Phys. **49**, 373 (2003).
[16] P. Salières, A. L'Huillier, Ph. Antoine, and M. Lewenstein, Adv. At., Mol., Opt. Phys. **41**, 83 (1999).
[17] R. Dörner, Th. Weber, W. Weckenbrock, A. Staudte, M. Hattass, R. Moshammer, J. Ullrich, and H. Schmidt-Böcking, Adv. At., Mol., Opt. Phys. **48**, 1 (2002).
[18] D. B. Milošević and F. Ehlotzky, Phys. Rev. A **58**, 2319 (1998).
[19] D. B. Milošević and F. Ehlotzky, Phys. Rev. A **65**, 042504 (2002).
[20] N. L. Manakov, A. F. Starace, A. V. Flegel, and M. V. Frolov, JETP Lett. **76**, 258 (2002).
[21] T. Brabec, M. Yu. Ivanov, and P. B. Corkum, Phys. Rev. A **54**, R2551 (1996).
[22] P. Hansch, M. A. Walker, and L. D. Van Woerkom, Phys. Rev. A **55**, R2535 (1997); M. P. Hertlein, P. H. Bucksbaum, and H. G. Muller, J. Phys. B **30**, L197 (1997); G. G. Paulus, F. Grasbon, H. Walther, R. Kopold, and W. Becker, Phys. Rev. A **64**, 021401(R) (2001).
[23] H. G. Muller and F. C. Kooiman, Phys. Rev. Lett. **81**, 1207 (1998); B. Borca, M. V. Frolov, N. L. Manakov, and A. F. Starace, *ibid.* **88**, 193001 (2002); S. V. Popruzhenko, Ph. A. Korneev, S. P. Goreslavski, and W. Becker, *ibid.* **89**, 023001 (2002); J. Wassaf, V. Véniard, R. Taïeb, and A. Maquet, *ibid.* **90**, 013003 (2003).
[24] G. F. Gribakin and M. Yu. Kuchiev, Phys. Rev. A **55**, 3760 (1997).
[25] R. Reichle, I. Yu. Kiyan, and H. Helm, J. Mod. Opt. **50**, 461 (2003).
[26] R. Reichle, H. Helm, and I. Yu. Kiyan, Phys. Rev. A **68**, 063404 (2003).
[27] B. M. Smirnov, *Physics of Atoms and Ions* (Springer, New York, 2003).
[28] G. F. Gribakin, V. K. Ivanov, A. V. Korol, and M. Yu. Kuchiev, J. Phys. B **32**, 5463 (1999).
[29] D. B. Milošević, A. Gazibegović-Busuladžić, and W. Becker, Phys. Rev. A **68**, 050702(R) (2003).
[30] N. L. Manakov and A. G. Fainshtein, Zh. Eksp. Teor. Fiz. **79**, 751 (1980); [Sov. Phys. JETP **52**, 382 (1980)].
[31] W. Becker, S. Long, and J. K. McIver, Phys. Rev. A **42**, 4416 (1990); **46**, R5334 (1992).
[32] N. L. Manakov, M. V. Frolov, B. Borca, and A. F. Starace, J. Phys. B **36**, R49 (2003).
[33] M. V. Frolov, N. L. Manakov, E. A. Pronin, and A. F. Starace, Phys. Rev. Lett. **91**, 053003 (2003).
[34] M. V. Frolov, N. L. Manakov, E. A. Pronin, and A. F. Starace, J. Phys. B **36**, L419 (2003).
[35] A. M. Perelomov, V. S. Popov, and M. V. Terent'ev, Zh. Eksp. Teor. Fiz. **51**, 309 (1966); [Sov. Phys. JETP **24**, 207 (1967)].
[36] R. Kopold, doctoral dissertation, Technische Universität München, 2001.
[37] B. Borca, M. V. Frolov, N. L. Manakov, and A. F. Starace, Phys. Rev. Lett. **87**, 133001 (2001).
[38] Note that, for given **p**, $n$ is determined via the $\delta$ function in Eq. (13).
[39] W. Becker, M. Kleber, A. Lohr, G. G. Paulus, H. Walther, and F. Zacher, Laser Phys. **8**, 56 (1998).
[40] R. Kopold, W. Becker, M. Kleber, and G. G. Paulus, J. Phys. B **35**, 217 (2002).
[41] V. K. Ivanov, J. Phys. B **32**, R67 (1999).
[42] S. J. Buckam and C. W. Clark, Rev. Mod. Phys. **66**, 539 (1994).
[43] G. G. Paulus, F. Zacher, H. Walther, A. Lohr, W. Becker, and M. Kleber, Phys. Rev. Lett. **80**, 484 (1998).
[44] I. Yu. Kiyan, Z. Ansari, B. Bergues, S. Beiser, M. Klaiber, and H. Helm, in Book of Abstracts, 13th International Laser Physics Workshop (LPHYS'04), Trieste, Italy, 2004 (unpublished), p. 116.
[45] G. G. Paulus, F. Grasbon, A. Dreischuh, H. Walther, R. Kopold, and W. Becker, Phys. Rev. Lett. **84**, 3791 (2000).
[46] P. Salières, B. Carré, L. Le Déroff, F. Grasbon, G. G. Paulus, H. Walther, R. Kopold, W. Becker, D. B. Milošević, A. Sanpera, and M. Lewenstein, Science **292**, 902 (2001).
[47] R. Kopold and W. Becker, in *Modern Challenges in Quantum Optics*, edited by M. Orszag and J. C. Retamal (Springer, Berlin, 2001), p. 294.
[48] D. B. Milošević and B. Piraux, Phys. Rev. A **54**, 1522 (1996).
[49] W. Becker, S. Long, and J. K. McIver, Phys. Rev. A **41**, 4112 (1990); **50**, 1540 (1994).
[50] D. B. Milošević, in *Super-Intense Laser-Atom Physics*, edited by B. Piraux and K. Rzążewski (Kluwer Academic Publishers, Dordrecht, 2001), p. 229.
[51] D. B. Milošević, J. Phys. B **33**, 2479 (2000).
[52] A. A. Radzig and B. M. Smirnov, *Reference Data on Atoms, Molecules and Ions* (Springer, Berlin, 1985).
[53] M. H. Mittleman and K. M. Watson, Phys. Rev. **113**, 198 (1959).
[54] F. Mandl, *Quantum Mechanics* (John Wiley & Sons, Chichester, 1992).
[55] *Computational Atomic Physics: Electron and Positron Collisions with Atoms and Ions*, edited by K. Bartschat (Springer, Berlin, 1996).
[56] J. E. Purcell, R. A. Berg, and A. E. S. Green, Phys. Rev. A **2**, 107 (1970).
[57] R. A. Berg, J. E. Purcell, and A. E. S. Green, Phys. Rev. A **3**, 508 (1971).
[58] A. E. S. Green, D. L. Sellin, and A. S. Zachor, Phys. Rev. **184**, 1 (1969).
[59] A. E. S. Green, D. E. Rio, and T. Ueda, Phys. Rev. A **24**, 3010

(1981).
[60] P. S. Ganas, J. D. Talman, and A. E. S. Green, Phys. Rev. A **22**, 336 (1980).
[61] P. S. Ganas, L. P. Gately, and T. Arakelian, Phys. Rev. A **30**, 2958 (1984).
[62] J. Neugebauer, M. Reiher, and J. Hinze, Phys. Rev. A **66**, 022717 (2002).